Atomic Layer Deposition of In_2O_3 Using Cyclopentadienyl Indium: A New Synthetic Route to Transparent Conducting Oxide Films

Jeffrey W. Elam,*,† Alex B. F. Martinson,†,‡ Michael J. Pellin,† and Joseph T. Hupp‡

Argonne National Laboratory, 9700 South Cass Avenue, Argonne, Illinois 60439, and Department of Chemistry, Northwestern University, Evanston, Illinois 60208

Received March 30, 2006. Revised Manuscript Received May 24, 2006

Indium oxide (In_2O_3) forms the basis for an important class of transparent conducting oxides that see wide use in optoelectronic devices, flat-panel displays, and photovoltaics. Here we present a new method for depositing In_2O_3 thin films by atomic layer deposition (ALD) using alternating exposures to cyclopentadienyl indium and ozone. Using a precursor vaporization temperature of 40 °C and deposition temperatures of 200−450 °C, we measure growth rates of 1.3−2.0 Å/cycle. A significant advantage of this synthesis route over previous techniques is the ability to conformally coat porous materials such as anodic aluminum oxide membranes. The deposited films are nanocrystalline, cubic phase In_2O_3 and are highly transparent and conducting. In situ quadrupole mass spectrometry and quartz crystal microbalance measurements elucidate the details of the In_2O_3 growth mechanism.

1. Introduction

In_2O_3 thin films have applications as transparent conducting oxides (TCOs),[1] gas sensors,[2−4] and catalysts.[5−9] For optimum performance, all of these applications require precise control over film thickness and composition, and some require the ability to coat high aspect ratio or porous materials.[2,5−7] In_2O_3 thin films can be deposited using a variety of methods including sputtering,[10,11] chemical vapor deposition,[12−15] and atomic layer deposition (ALD).[16−20] Of these techniques, ALD shows significant promise as this method affords excellent control over both the thickness and the composition of the deposited film.[21] Most importantly, ALD offers unmatched conformality that enables the coating of porous materials with aspect ratios in excess of 1000.[22−24]

Previously, In_2O_3 ALD has been accomplished using $InCl_3$ with either H_2O[16] or H_2O_2[19] as the oxygen source. Although useful for coating planar surfaces, this method suffers from several limitations. First, the $InCl_3$ chemistry requires high growth temperatures of ∼300−500 °C and yields a low growth rate of only 0.25−0.40 Å/cycle. In addition, the $InCl_3$ has a very low vapor pressure and must be heated to 285 °C just to saturate a planar surface. Furthermore, the corrosive HCl byproduct can damage the deposition equipment. But the greatest limitation of the $InCl_3/H_2O$ method, especially for coating nanoporous materials, is that $InCl_3$ can etch the deposited In_2O_3.[16] Nanoporous materials require very long precursor exposures that are likely to completely remove the In_2O_3 from the outer portions of the nanoporous substrate.

The primary goal of this study was to develop an improved ALD process for In_2O_3 that allows the coating of nanoporous materials. A number of alternate precursors have been investigated previously including β-diketonates[20] ($In(hfac)_3$ (hfac = hexafluoropentadionate), $In(thd)_3$ (thd = 2,2,6,6-

* To whom correspondence should be addressed. E-mail: jelam@anl.gov.
† Argonne National Laboratory.
‡ Northwestern University.

(1) Edwards, P. P.; Porch, A.; Jones, M. O.; Morgan, D. V.; Perks, R. M. *Dalton Trans.* **2004**, 2995.
(2) Kiriakidis, G.; Suchea, M.; Christoulakis, S.; Katsarakis, N. *Rev. Adv. Mater. Sci.* **2005**, *10*, 215.
(3) Golovanov, V.; Maeki-Jaskari, M. A.; Rantala, T. T.; Korotcenkov, G.; Brinzari, V.; Cornet, A.; Morante, J. *Sens. Actuators, B* **2005**, *106*, 563.
(4) Korotcenkov, G.; Brinzari, V.; Cerneavschi, A.; Ivanov, M.; Golovanov, V.; Cornet, A.; Morante, J.; Cabot, A.; Arbiol, J. *Thin Solid Films* **2004**, *460*, 315.
(5) Gervasini, A.; Perdigon-Melon, J. A.; Guimon, C.; Auroux, A. *J. Phys. Chem. B* **2006**, *110*, 240.
(6) Perdigon-Melon, J. A.; Gervasini, A.; Auroux, A. *J. Catal.* **2005**, *234*, 421.
(7) Li, J.; Hao, J.; Cui, X.; Fu, L. *Catal. Lett.* **2005**, *103*, 75.
(8) Zhu, T.; Hao, J.; Fu, L.; Wang, J.; Li, J.; Liu, Z.; Cui, X. *Huanjing Kexue* **2004**, *25*, 26.
(9) Ren, L.; Zhang, T.; Xu, C.; Lin, L. *Top. Catal.* **2004**, *30/31*, 55.
(10) Qiao, Z.; Mergel, D. *Thin Solid Films* **2005**, *484*, 146.
(11) Nishimura, E.; Ohkawa, H.; Sato, Y.; Song, P.-K.; Shigesato, Y. *Shinku* **2004**, *47*, 796.
(12) Kim, H. W.; Kim, N. H.; Myung, J. H. *J. Mater. Sci.* **2005**, *40*, 4991.
(13) Ni, J.; Yan, H.; Wang, A.; Yang, Y.; Stern, C. L.; Metz, A. W.; Jin, S.; Wang, L.; Marks, T. J.; Ireland, J. R.; Kannewurf, C. R. *J. Am. Chem. Soc.* **2005**, *127*, 5613.
(14) Kim, N. H.; Myung, J. H.; Kim, H. W.; Lee, C. *Phys. Status Solidi A* **2005**, *202*, 108.
(15) Girtan, M.; Folcher, G. *Surf. Coat. Technol.* **2003**, *172*, 242.
(16) Asikainen, T.; Ritala, M.; Leskela, M. *J. Electrochem. Soc.* **1994**, *141*, 3210.
(17) Asikainen, T.; Ritala, M.; Leskelae, M. *J. Electrochem. Soc.* **1995**, *142*, 3538.
(18) Asikainen, T.; Ritala, M.; Leskelae, M. *Vacuum* **1995**, *46*, 887.
(19) Ritala, M.; Asikainen, T.; Leskela, H. *Electrochem. Solid State Lett.* **1998**, *1*, 156.
(20) Ritala, M.; Asikainen, T.; Leskelae, M.; Skarp, J. *Mater. Res. Soc. Symp. Proc.* **1996**, *426*, 513.
(21) Ritala, M.; Leskela, M. *Handb. Thin Film Mater.* **2002**, *1*, 103.
(22) Pellin, M. J.; Stair, P. C.; Xiong, G.; Elam, J. W.; Birrell, J.; Curtiss, L.; George, S. M.; Han, C. Y.; Iton, L.; Kung, H.; Kung, M.; Wang, H. H.; *Catal. Lett.* **2005**, *102*, 127.
(23) Kucheyev, S. O.; Biener, J.; Wang, Y. M.; Baumann, T. F.; Wu, K. J.; van Buuren, T.; Hamza, A. V.; Satcher, J. H.; Elam, J. W.; Pellin, M. J. *Appl. Phys. Lett.* **2005**, 86.
(24) Elam, J. W.; Routkevitch, D.; Mardilovich, P. P.; George, S. M. *Chem. Mater.* **2003**, *15*, 3507.

10.1021/cm060754y CCC: $33.50
Published on Web 07/01/2006

tetramethyl-3,5-heptanedioneate), and $In(acac)_3$ (acac = 2,4-pentanedionate)) and trimethyl indium,[25] ($In(CH_3)_3$). Unfortunately, these efforts were unsuccessful. No growth was observed using β-diketonates with water or hydrogen peroxide, while trimethyl indium did not yield self-limiting growth. In this paper we describe a new method for In_2O_3 ALD using cyclopentadienyl indium(I) (InCp) and ozone. A related compound, pentamethylcyclopentadienyl indium-(I), has been used previously for InP chemical vapor deposition.[26] We utilize in situ quadrupole mass spectrometer (QMS) and quartz crystal microbalance (QCM) measurements to understand the growth mechanism. Next, we deposit In_2O_3 films on Si(100) and glass substrates and analyze the films using spectroscopic ellipsometry, X-ray powder diffraction (XRD), four-point probe resistivity, atomic force microscopy (AFM), UV−visible absorption spectroscopy, and scanning electron microscopy (SEM). These analyses reveal that cubic phase, nanocrystalline In_2O_3 is deposited at a growth rate of 2.0 Å/cycle. Finally, we apply this technique to conformally coat nanoporous anodic aluminum oxide (AAO) membranes.

2. Experimental Section

The ALD films were deposited in a custom viscous flow reactor similar in design to those that have been described previously.[27] Briefly, a stainless steel flow tube with an inside diameter of 5 cm houses substrates for film growth as well as the QCM. Ultrahigh purity nitrogen carrier gas continuously passes through the flow tube at a mass flow rate of 360 sccm and a pressure of 1 Torr. A constant reactor temperature is maintained by four separate temperature controllers connected to resistive heating elements attached to the outside of the reactor. The four heating zones create a uniform temperature profile along the length of the flow tube to reduce the influence of temperature transients on the QCM measurements.[28]

In_2O_3 ALD was performed using alternating exposures to cyclopentadienyl indium(I) (InCp, Strem, electronic grade 99.999+% In) and ozone. The InCp is held in a stainless steel bubbler maintained at 40 °C, and the tubing connecting the bubbler to the ALD reactor is maintained at 200 °C to prevent the deposition of InCp on the reactor walls. Ultrahigh purity nitrogen (99.999%) at a mass flow rate of 60 sccm was sent through the bubbler during the InCp exposures and was diverted to bypass the bubbler following the InCp exposures. The ozone was produced using a commercial ozone generator (Ozone Engineering L11) using a feed of ultrahigh purity oxygen at a flow rate of 400 sccm to produce ~10% ozone in oxygen. We also attempted In_2O_3 ALD using β-diketonate precursors with ozone. The β-diketonate precursors used were $In(hfac)_3$ (Gelest) and $In(acac)_3$ (Gelest). Additional oxygen sources evaluated for In_2O_3 ALD included deionized water (18 MΩ cm), hydrogen peroxide (30% solution in water, Aldrich), ultrahigh purity oxygen, and nitrous oxide (Aldrich, 99%).

The ALD timing sequences can be expressed as t1−t2−t3−t4, where t1 is the exposure time for the first precursor, t2 is the purge time following the first exposure, t3 is the exposure time for the second precursor, t4 is the purge time following the exposure to the second precursor, and all units are given in seconds (s). The timing sequence for In_2O_3 ALD was typically 2−4−2−2 s.

A QCM was installed in the ALD reactor in place of substrates enabling in situ measurements during the In_2O_3 growth. These measurements utilized a Maxtek BSH-150 bakeable sensor and AT-cut quartz sensor crystals with a polished front surface obtained from the Colorado Crystal Corp., part no. CCAT1BK-1007-000. The QCM measurements were made using a Maxtek TM400 film thickness monitor interfaced to a personal computer. In addition, the ALD reactor was equipped with a QMS (Stanford Research Systems RGA300) located downstream of the QCM in a differentially pumped chamber separated from the reactor tube by a 35 μm orifice and evacuated using a 50 L/s turbomolecular pump.

In_2O_3 ALD films were deposited on 1 cm × 2 cm Si(100) and glass substrates. Prior to loading, the substrates were ultrasonically cleaned in acetone and then 2-propanol and blown dry using nitrogen. After loading, the substrates were allowed to outgas in the ALD reactor for 10 min at the deposition temperature (typically 250 °C) in 1 Torr of flowing ultrahigh purity nitrogen. Next, the substrates were cleaned in situ using a 60 s exposure to 10% ozone in oxygen at a pressure of 2 Torr and a mass flow rate of 400 sccm. We observed a reactor conditioning effect in which the thicknesses of the In_2O_3 films deposited immediately following Al_2O_3 growth were thinner than expected. To compensate for this effect, we always deposited an In_2O_3 buffer layer on the inside of the reactor using ~100 $InCp/O_3$ cycles following depositing of a different material.

SEM images were acquired using a Hitachi S4700 scanning electron microscope with a field emission gun electron beam source, secondary electron and backscattered electron detectors, and an energy dispersive analysis of X-rays (EDAX) detector for elemental analysis. AFM measurements were performed on a Digital Instruments Dimension 3000 with a NanoScope IIIa controller operated in tapping mode. XRD measurements were taken on a Rigaku Miniflex Plus diffractometer. Ellipsometric measurements of the In_2O_3 films deposited on Si(100) surfaces were performed using a J. A. Woolam Co. M2000 variable angle spectroscopic ellipsometer using a table of refractive indexes for In_2O_3 supplied with the instrument. Optical absorption spectra were acquired from ALD In_2O_3 films deposited on glass using the M2000 operated in transmission mode and were fit to a model using the same In_2O_3 optical constants. AAO membranes (Whatman Anodisc 13) with pore diameters of 200 nm and a membrane thickness of 70 μm were also coated by In_2O_3. Prior to SEM analysis, cleaved cross sections of the membranes were embedded in conducting epoxy and polished with progressively finer diamond polishing compound ending with 0.25 μm.

3. Results and Discussion

(A) Initial Studies Using β-Diketonates. A previous study measured virtually no In_2O_3 growth using indium β-diketonates ($In(acac)_3$, $In(hfac)_3$, and $In(thd)_3$) with either water or hydrogen peroxide as the oxygen source.[20] The lack of growth was attributed to the very low reactivity of these β-diketonate precursors to the In_2O_3 surface; however, ALD with ozone was not tested in this previous study. Ozone is often successful in ALD with β-diketonates,[29−31] so we

(25) Ott, A. W.; Johnson, J. M.; Klaus, J. W.; George, S. M. *Appl. Surf. Sci.* **1997**, *112*, 205.
(26) Haugan, H. J.; Yu, W.; Lee, S. T.; Petrou, A.; McCombe, B. D.; Brewer, K. S.; Lees, J. F.; Beachley, O. T. *J. Cryst. Growth* **2002**, *244*, 157.
(27) Elam, J. W.; Groner, M. D.; George, S. M. *Rev. Sci. Instrum.* **2002**, *73*, 2981.
(28) Elam, J. W.; Pellin, M. J. *Anal. Chem.* **2005**, *77*, 3531.
(29) Paivasaari, J.; Putkonen, M.; Sajavaara, T.; Niinisto, L. *J. Alloys Compd.* **2004**, *374*, 124.
(30) Myllymaki, P.; Nieminen, M.; Niinisto, J.; Putkonen, M.; Kukli, K.; Niinisto, L. *J. Mater. Chem.* **2006**, *16*, 563.

Table 1. Growth Rate for In_2O_3 Films Deposited on Si(100) Substrates Using 100 Cycles of InCp and Different Oxygen Sources at 250−275 °C

oxygen source	In_2O_3 growth rate thickness (Å/cycle)
ozone	1.3
oxygen	0.16
water	0.068
hydrogen peroxide	0.039
nitrous oxide	0.065

initially tried using $In(acac)_3$ and $In(hfac)_3$ with O_3. In situ QCM experiments performed at 150−300 °C on a previously deposited ALD Al_2O_3 surface consistently yielded 0.3−1.0 Å of In_2O_3 during the first ALD cycle but little or no growth afterward. This suggests that the reactivity of the indium β-diketonates is relatively high on Al_2O_3 but too low on the In_2O_3 to support growth even using O_3. We attempted to deposit In_2O_3 films on Si(100) and glass substrates using $In(hfac)_3/O_3$ at a higher temperature of 350−500 °C. When an $In(hfac)_3$ bubbler temperature of 160 °C was used, the growth rate increased sharply with temperature from 0.03 Å/cycle at 350 °C to 0.51 Å/cycle at 500 °C, but the results were erratic. These difficulties may result from thermal decomposition of the $In(hfac)_3$ inside the reactor tube or in the bubbler or possibly sintering of the solid indium compound.

After our lack of success with $In(acac)_3$ and $In(hfac)_3$, we shifted our attention to InCp. Our initial measurements were encouraging as we discovered that we could deposit In_2O_3 films using $InCp/O_3$. Preliminary experiments were performed to determine the appropriate InCp bubbler temperature. In_2O_3 films were deposited using the timing sequence 2−2−1−2 on Si(100) substrates at 250 °C for 100 cycles while varying the InCp bubbler temperature between 30 and 60 °C. These measurements demonstrated that the InCp growth rate was nearly constant using bubbler temperatures above 40 °C. Using the Baratron pressure gauge, we measured a vapor pressure for InCp of 0.1 Torr at 40 °C. We tried using InCp with other oxygen sources, but the growth rates were substantially lower as shown in Table 1. It is curious that the water did not allow growth considering that H_2O is a typical oxygen source in metal oxide film ALD utilizing cyclopentadienyl precursors.[30,32,33] It may be that the more powerful oxidizing agent, O_3, is necessary to oxidize the In from +1 to +3.

(B) In Situ Measurements during In_2O_3 ALD. In situ QCM and QMS measurements were used to investigate the mechanism for In_2O_3 ALD using InCp and O_3. These measurements were performed at 250 °C using the timing sequence 2−5−2−15. The In_2O_3 ALD process can be described by a generalized reaction scheme:

$$* + \mathrm{InCp} \rightarrow \mathrm{InCp}_x* + (1 - x)\mathrm{products} \quad (1)$$

$$\mathrm{InCp}_x* + \mathrm{oxidant} \rightarrow \mathrm{InO}_{1.5}* + (x)\mathrm{products} \quad (2)$$

In these reactions, the surface species are designated with an asterisk and x is the fraction of Cp ligands remaining on the surface following each InCp exposure. The gas-phase products, the initial reactive sites, and the oxidant are all left unspecified but will be determined from the in situ measurements.

QMS measurements were performed to determine the gas-phase products of the InCp and ozone half-reactions. Representative QMS data recorded during the InCp and O_3 half-reactions are shown in Figure 1a,b, respectively. As shown in Figure 1a, a peak at $m = 66$ appears during the InCp half-reaction, but not during the O_3 half-reaction. When the InCp exposure follows an O_3 exposure, the $m = 66$ peak has a sharp spike at the leading edge followed by a smaller plateau that persists as long as the InCp dosing valve is held open as illustrated by the first two ALD cycles in the figure. However, if no O_3 exposure precedes the InCp exposure, the sharp spike in the $m = 66$ peak is absent as shown by the final two ALD cycles in Figure 1a. From these observations we conclude that the sharp feature represents a gas-phase product of reaction 1, while the smaller plateau is simply decomposition of the InCp precursor in the QMS.

Similarly, we see a sharp spike in the $m = 44$ signal coincident with the O_3 exposures that are preceded by InCp exposures (Figure 1b); however, this spike is not seen when the InCp exposures are absent. Consequently, we conclude that $m = 44$ is a gas-phase product of reaction 2. The small peak in the $m = 44$ data coincident with the InCp exposures is present whether or not the InCp exposure is preceded by an O_3 exposure, and therefore this is a crack of InCp rather than a reaction product. The large, slow transient feature in the $m = 44$ signal that appears during the purge cycle of each O_3 exposure results from a CO_2 impurity in the ultrahigh purity oxygen which is pumped slowly by our system.

By collecting QMS data over the mass range 12−115 amu, we discovered that $m = 44$ (CO_2) is the only product of the O_3 reaction, while the InCp reaction yields the following products (and relative abundances): $m = 66$ (100), 65 (67), 39 (53), and 40 (33). This mass pattern matches closely the fragmentation pattern for cyclopentadiene (C_5H_6).[34] We also looked for the cyclopentadienyl dimer at $m = 132$, but we found none. It is surprising that we do not observe water during the O_3 half-reaction. One explanation is that the hydrogen from the Cp ligands in reaction 2 remains on the surface as hydroxyl (OH) groups that subsequently react with InCp to form HCp (cyclopentadiene, $m = 66$). This would explain why no $m = 18$ is observed in reaction 2, while the main product from reaction 1 is $m = 66$ rather than $m = 65$.

The ratio of gas-phase products measured during the InCp and O_3 half-reactions can be used to calculate x in eqs 1 and 2. By integrating the product mass peaks observed during the InCp exposures and correcting for variations in electron multiplier gain, quadrupole transmission, and ionization efficiency, we calculate that the amount of Cp released during eq 1 is (in arbitrary units) $1 - x = 15$. Similarly, after correcting for the relative effusion rate of CO_2 versus

(31) Niinisto, J.; Petrova, N.; Putkonen, M.; Niinisto, L.; Arstila, K.; Sajavaara, T. *J. Cryst. Growth* **2005**, *285*, 191.
(32) Paivasaari, J.; Niinisto, J.; Arstila, K.; Kukli, K.; Putkonen, M.; Niinisto, L. *Chem. Vap. Deposition* **2005**, *11*, 415.
(33) Niinisto, J.; Putkonen, M.; Niinisto, L.; Stoll, S. L.; Kukli, K.; Sajavaara, T.; Ritala, M.; Leskela, M. *J. Mater. Chem.* **2005**, *15*, 2271.
(34) *Eight Peak Index of Mass Spectra*; Mass Spectometry Data Centre, The Royal Society of Chemistry: Cambridge, U.K., 1991.

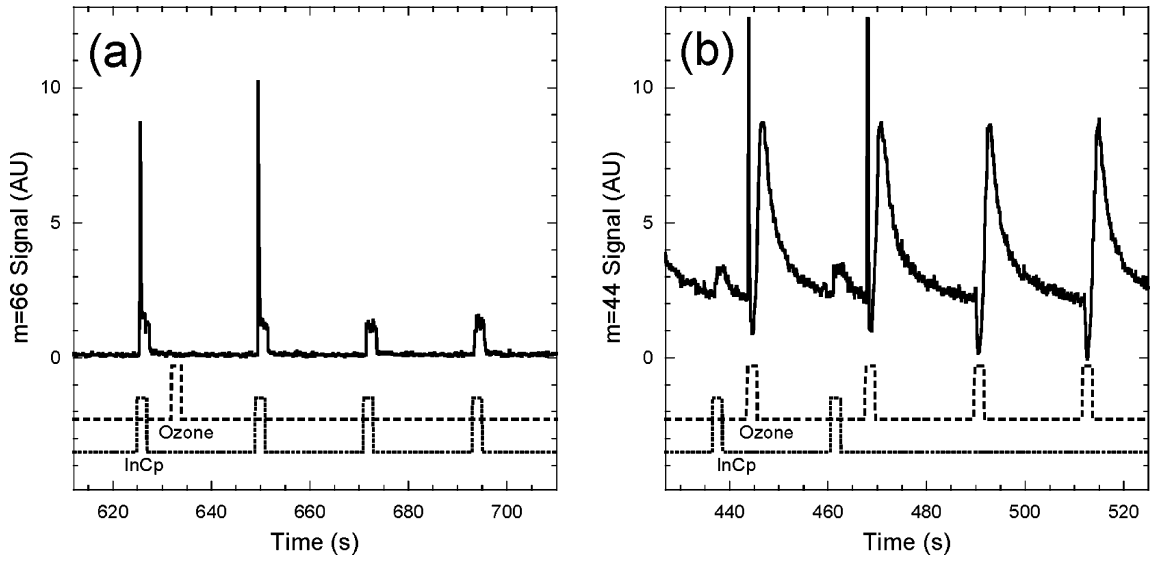

Figure 1. (a) QMS signal for $m = 66$ (cyclopentadiene, solid line) versus time during alternating exposures to InCp (dotted line) and O_3 (dashed line) at 250 °C using the timing sequence 2−5−2−15. (b) QMS signal for $m = 44$ (CO_2) recorded using the same conditions as in part a.

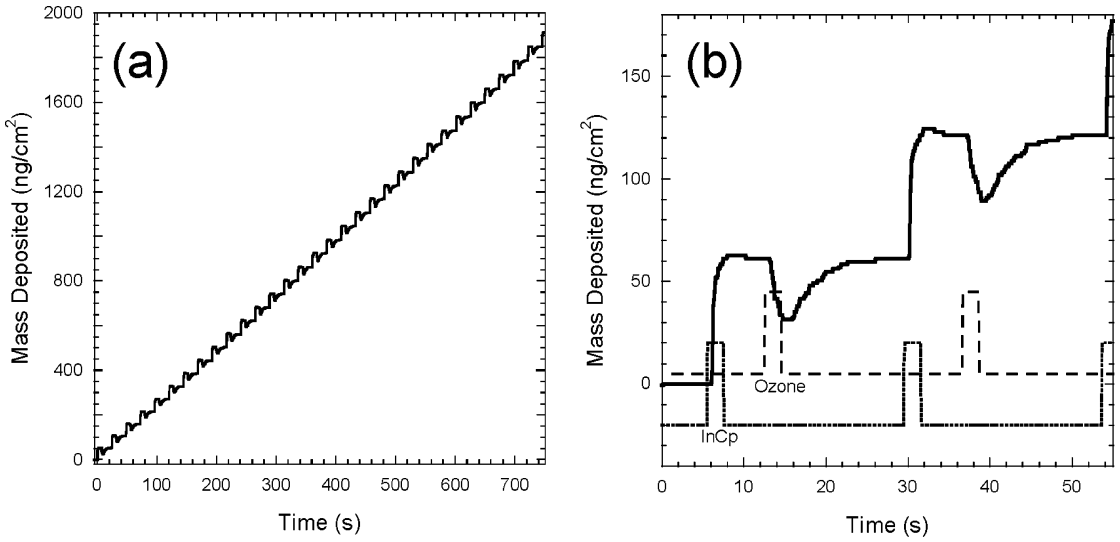

Figure 2. (a) QCM signal versus time during alternating exposures to InCp and O_3 at 250 °C using the timing sequence 2−5−2−15. (b) Expanded view showing correlation between QCM signal (solid line) and exposures to InCp (dotted line) and O_3 (dashed line).

cyclopentadiene, the amount of CO_2 released during eq 2 is $5x = 13.8$, where the quantity $5x$ accounts for the fact that five CO_2 molecules are released from each Cp ligand. Combining these expressions, $(1 - x)/(5x) = 1.09$ so that $x = 0.15$.

Figure 2a shows the QCM data recorded simultaneously with the QMS measurements demonstrating that alternating InCp/O_3 exposures results in a linear mass increase versus time. The slope of the data in Figure 2a yields a net mass change of 55 ng/cm^2/cycle. Assuming a bulk density for In_2O_3 of 7.19 g/cm^2, this corresponds to a growth rate of 0.76 Å/cycle. As described in the next section, this growth rate is lower than the 1.3−2.0 Å/cycle measured on Si(100) substrates. This difference arises because the QCM is located ~33 cm downstream from the substrates where the O_3 concentration is lower.

Figure 2b shows an expanded view of the QCM data for two ALD cycles. There is an abrupt mass increase during each InCp exposure and a transient mass decrease coincident with each O_3 exposure followed by a slow increase such that the net mass change produced by the O_3 exposures is almost zero. We attribute the apparent mass decrease during the O_3 exposures to a transient heating of the QCM produced by the thermal decomposition of O_3 or the oxidation of the Cp ligands.[28] The mass changes produced by the individual half-reactions can predict the fraction of Cp ligands remaining on the surface after the InCp exposures. Using the relationship $R = \Delta m/\Delta m_2$, where Δm is the mass change from one complete cycle and Δm_2 is the mass change during reaction 1, we calculate from eqs 1 and 2 and the atomic masses that $\Delta m(InO_{1.5}) = 139$ and $\Delta m_2[In + (x)Cp] = 115 + 65x$ so that $R = 139/(115 + 65x)$. From Figure 1a, $R = 1.0$ so that $x = 0.37$ which implies that, on average, 37% of the Cp ligands remain on the surface after reaction 1. This value is somewhat higher than the value $x = 0.15$ calculated from the QMS data. This difference probably arises from uncertainties in the QMS parameters used to calculate the cyclopentadiene and CO_2 concentrations or from inaccuracies

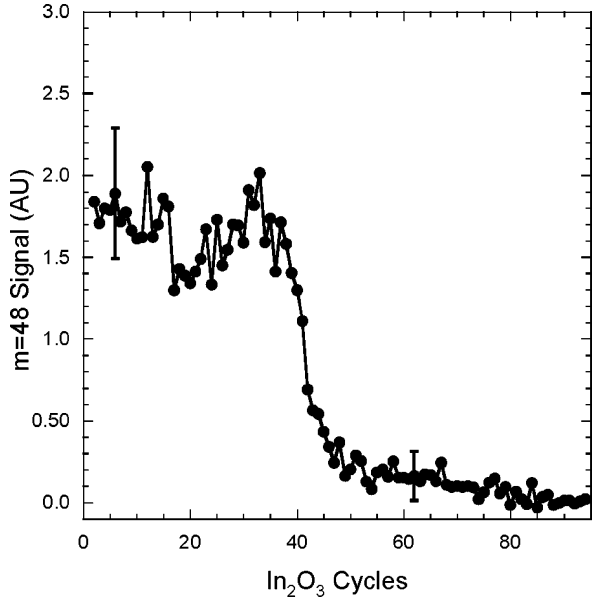

Figure 3. QMS signal for $m = 48$ (ozone) versus number of $InCp/O_3$ cycles using the timing sequence 2−5−2−15 at 250 °C after previously coating the ALD reactor with Al_2O_3.

in the QCM data caused by the temperature-induced transient feature during the O_3 exposures. Nevertheless, the primary conclusion from the QCM data is the same as from the QMS data: a majority of the Cp ligands are lost during the InCp exposures, and the small fraction remaining is subsequently removed during the following O_3 exposure.

One additional finding from the in situ measurements is that the reactive oxygen species during the In_2O_3 ALD is most probably oxygen radicals formed by the thermal decomposition of ozone ($O_3 \rightarrow O_2 + O$). This process occurs primarily on the In_2O_3 surface but also to a lesser degree on other surfaces (e.g., Al_2O_3) or possibly in the gas phase. The In_2O_3 growth rate drops off abruptly at 200 °C to nearly zero (Figure 7) suggesting that we must exceed a threshold temperature for ozone decomposition to enable In_2O_3 growth. This interpretation is supported by the observation that the $m = 48$ QMS signal from ozone is ∼10× larger at temperatures below 200 °C. Furthermore, In_2O_3 appears to catalyze O_3 decomposition more efficiently than Al_2O_3 or gas-phase decomposition. Figure 3 demonstrates that when we first execute $InCp/O_3$ cycles following Al_2O_3 growth, the $m = 48$ signal is initially high but decreases nearly to zero following 40−50 In_2O_3 cycles. Moreover, in situ QCM measurements reveal that the In_2O_3 growth is initially inhibited following Al_2O_3 growth. Taken together, these results suggest that ozone decomposes on the growing surface to form a more active oxidizing species. This species is most likely a surface-bound oxygen radical or possibly a surface peroxide.[35]

To summarize the in situ measurements, we can rewrite eqs 1 and 2 with the unknown surface species, gaseous products, and oxidant filled in:

$$5OH^* + O^* + 6InCp \rightarrow 5O{-}In^* + O{-}In(Cp)^* + 5C_5H_6 \quad (3)$$

$$5O{-}In^* + O{-}In(Cp)^* + 19O^* \rightarrow 5O{-}In(O)_{0.5}{-}OH^* + O{-}In(O)_{1.5}{}^* + 5CO_2 \quad (4)$$

In reaction 3, the initial reactive sites are five OH groups and one surface oxygen species. Six InCp molecules react with the surface liberating five cyclopentadiene molecules and leaving one Cp ligand on the surface. In reaction 4, surface-bound oxygen species formed by the decomposition of O_3 release the carbon from the remaining Cp ligand as five CO_2, but the hydrogen atoms remain to reform five new hydroxyl groups. Consequently, reaction 4 regenerates the initial surface and forms In_2O_3 with the proper stoichiometry, In/O = 1:1.5. Equations 3 and 4 yield $x = 1/6 = 0.17$, which is in the range of $x = 0.15-0.37$ determined from the in situ measurements. Although somewhat speculative, this mechanism has the appeal that the single remaining Cp ligand will exactly balance the five OH groups so that no hydrogen-containing products are released during the O_3 reaction. Although the indium oxidation state is not explicit in eqs 3 and 4, the conversion from In^{1+} to In^{3+} probably occurs mostly during the ozone step. In situ measurements using infrared absorption spectroscopy[36] could verify the existence of OH groups following the O_3 exposures. If oxygen radicals are indeed the active oxidizing species in this process, then substituting an oxygen plasma[37] in place of the O_3 may allow In_2O_3 growth below 200 °C.

(C) Growth of In_2O_3 Films. Following the in situ measurements, we proceeded with In_2O_3 deposition on Si-(100) and glass substrates to study the In_2O_3 growth. Figure 4a shows the results of uptake measurements made while varying the exposure time to InCp using the timing sequence x−2−2−2. This figure demonstrates self-limiting behavior for InCp for exposure times of ∼2 s. Figure 4b shows a similar graph exploring the effect of increasing ozone exposures using the timing sequence 2−2−x−2 and demonstrates self-limiting In_2O_3 growth for ozone exposure times beyond ∼2 s. Increasing the InCp and O_3 purge times did not affect the In_2O_3 growth rates, indicating that purge times ≥2 s are sufficient to avoid mixing the precursors. For the remainder of the measurements, a timing sequence of 2−4−2−2 was used unless otherwise noted.

Figure 5 reveals nearly linear In_2O_3 growth over the range of 50−1000 $InCp/O_3$ cycles at an average growth rate of 2.0 Å/cycle. Figure 6 demonstrates that the In_2O_3 growth rate actually increases somewhat with the number of cycles from 1.3 to 2.0 Å/cycle over the range of 50−2000 ALD cycles. This increase probably results from an increase in surface area with the evolution and growth of the In_2O_3 nanocrystals. Gradual changes in ALD growth rates have been observed previously for nanocrystalline materials in which the morphology or crystal size evolves with film

(35) Li, W.; Gibbs, G. V.; Oyama, S. T. *J. Am. Chem. Soc.* **1998**, *120*, 9041.
(36) Ferguson, J. D.; Weimer, A. W.; George, S. M. *Appl. Surf. Sci.* **2000**, *162*, 280.
(37) Niskanen, A.; Arstila, K.; Ritala, M.; Leskela, M. *J. Electrochem. Soc.* **2005**, *152*, F90.

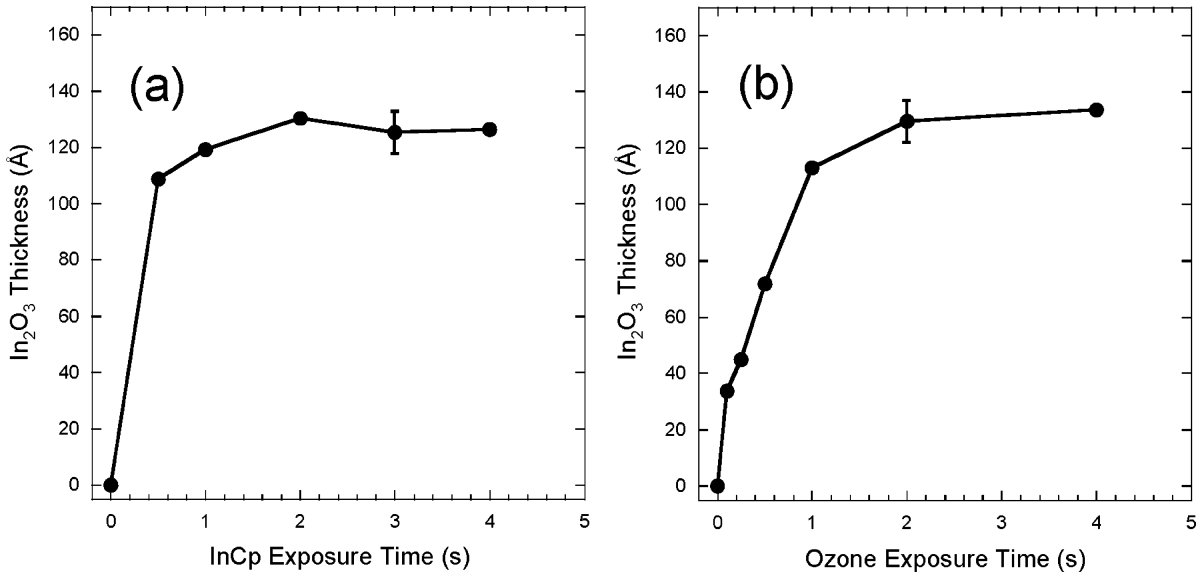

Figure 4. (a) In_2O_3 growth rate versus InCp exposure time measured by ellipsometry for films deposited on Si(100) using the timing sequence $x-2-2-2$ at 250 °C. (b) In_2O_3 growth rate versus O_3 exposure time measured similar to Figure 4a using the timing sequence $2-2-x-2$.

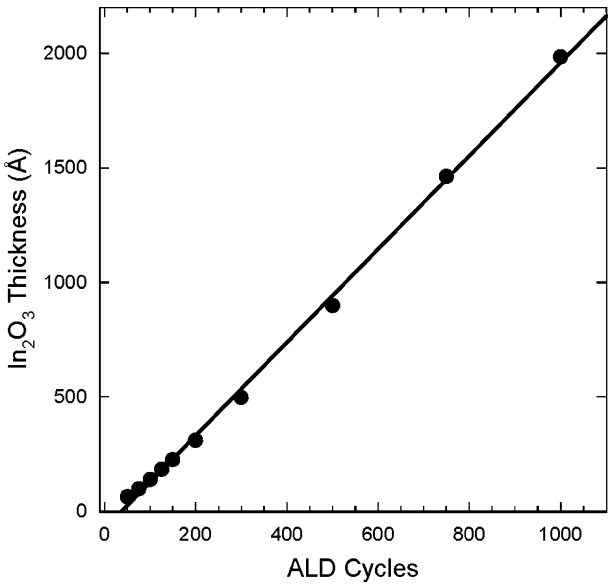

Figure 5. In_2O_3 thickness versus number of InCp/O_3 cycles measured by ellipsometry for films deposited on Si(100) using the timing sequence $2-4-2-2$ at 275 °C.

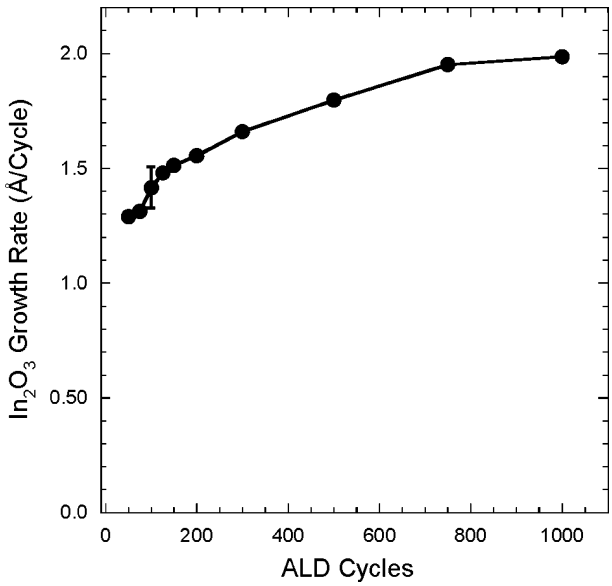

Figure 6. In_2O_3 growth rate versus number of cycles derived from Figure 5.

thickness.[38,39] The effect of deposition temperature on the In_2O_3 growth is shown in Figure 7. Surprisingly, the In_2O_3 growth rate drops precipitously below 200 °C. We believe that 200 °C is the threshold temperature below which ozone no longer decomposes to form oxygen radicals necessary for In_2O_3 growth. Between 200 and 450 °C, the In_2O_3 growth rate is nearly constant at 1.2−1.4 Å/cycle. At 500 °C, it was difficult to control the film thickness because most of the InCp decomposed at the leading edge of the sample holder in the reactor.

We also examined the variation in In_2O_3 film thickness along the flow direction of the reactor. Using the $2-4-2-2$ timing sequence, the film thickness was constant for the first ~15 cm of the reactor, after which the film thickness dropped off by 53% over 22 cm. The film uniformity improved using 15 s of O_3 exposure times so that the thickness decreased by only 33% over 22 cm, but the thickness variation was unaffected using longer InCp exposure times. We attribute this behavior to the depletion of ozone along the flow direction of the reactor.

The results of the film growth studies are summarized in Table 2 where we compare the InCp/O_3 process with the existing In_2O_3 ALD process using $InCl_3/H_2O_2$.

(D) Properties of In_2O_3 Films. Figure 8 shows an XRD measurement for a 176 nm film deposited on glass at 275 °C. The peaks in Figure 8 match closely cubic, polycrystalline In_2O_3 (PDF number 00-006-0416) as illustrated by the Miller indices in the figure. In agreement with the XRD, the AFM image in Figure 9 reveals a relatively rough,

(38) Elam, J. W.; Sechrist, Z. A.; George, S. M. *Thin Solid Films* **2002**, *414*, 43.
(39) Ritala, M.; Leskela, M.; Nykanen, E.; Soininen, P.; Niinisto, L. *Thin Solid Films* **1993**, *225*, 288.

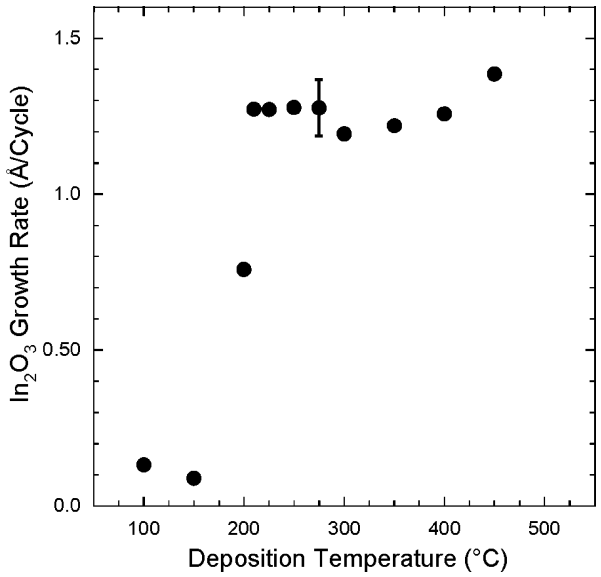

Figure 7. In_2O_3 growth rate versus deposition temperature measured by ellipsometry for films deposited on Si(100) using 100 In_2O_3 ALD cycles with the timing sequence 2−4−2−2.

Table 2. Comparison of $InCl_3$ and InCp Precursors for In_2O_3 ALD

	indium precursor	
	$InCl_3$	InCp
oxygen source	H_2O_2	O_3
ALD temperature window (°C)	300−500	200−450
precursor temperature (°C)	285	40
growth rate (Å/cycle)	0.40	2.0
precursor etching?	yes	no
reference	19	this work

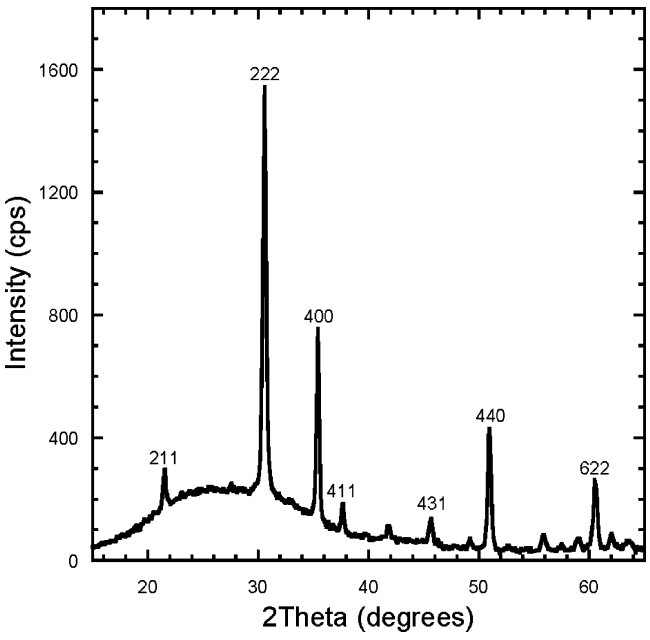

Figure 8. X-ray diffractogram recorded from 173 nm ALD In_2O_3 film deposited on glass using the timing sequence 2−4−2−4 at 275 °C.

nanocrystalline topography for a 100 nm In_2O_3 film deposited on Si(100). This image has a *z* range of 30 nm and yields a root-mean-squared (RMS) roughness of $R = 3.96$ nm for the 1×1 μm scan. The RMS roughness increases somewhat to $R = 4.9$ and 5.8 nm for scan sizes of 2×2 and 10×10 μm, respectively. Nanocrystals with a lateral dimension of 50−100 nm are evident in the plan view SEM image for the 100 nm In_2O_3 sample on Si(100) shown in Figure 10.

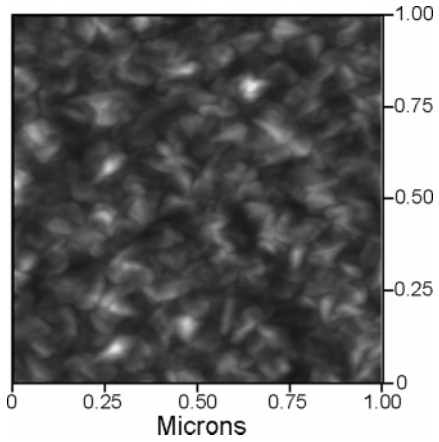

Figure 9. Tapping-mode AFM image recorded from 100 nm ALD In_2O_3 film deposited on Si(100) using the timing sequence 2−4−2−4 at 275 °C. The contrast scale for this image is 30 nm, and the RMS roughness is 3.96 nm.

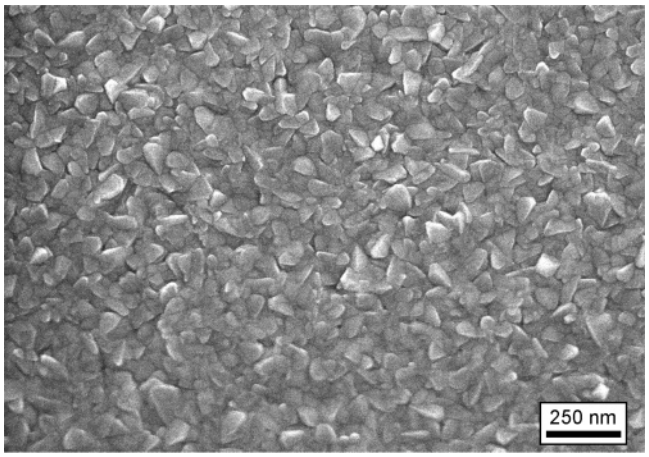

Figure 10. Plan view SEM image of 100 nm ALD In_2O_3 film deposited on Si(100) using the timing sequence 2−4−2−4 at 275 °C.

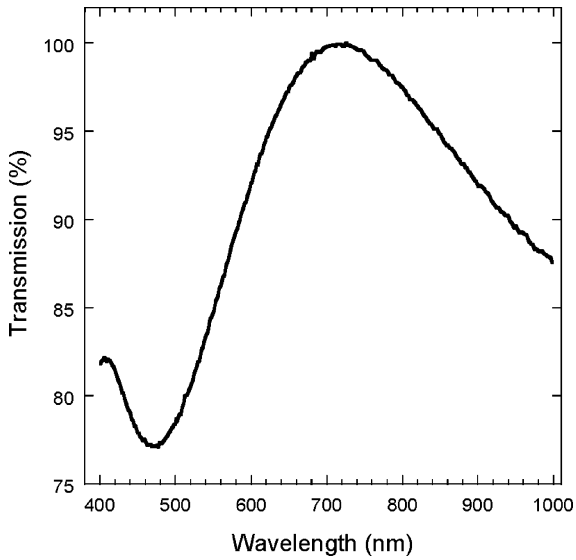

Figure 11. Optical transmission spectrum for 173 nm ALD In_2O_3 film deposited on glass using the timing sequence 2−4−2−4 at 275 °C referenced to uncoated glass.

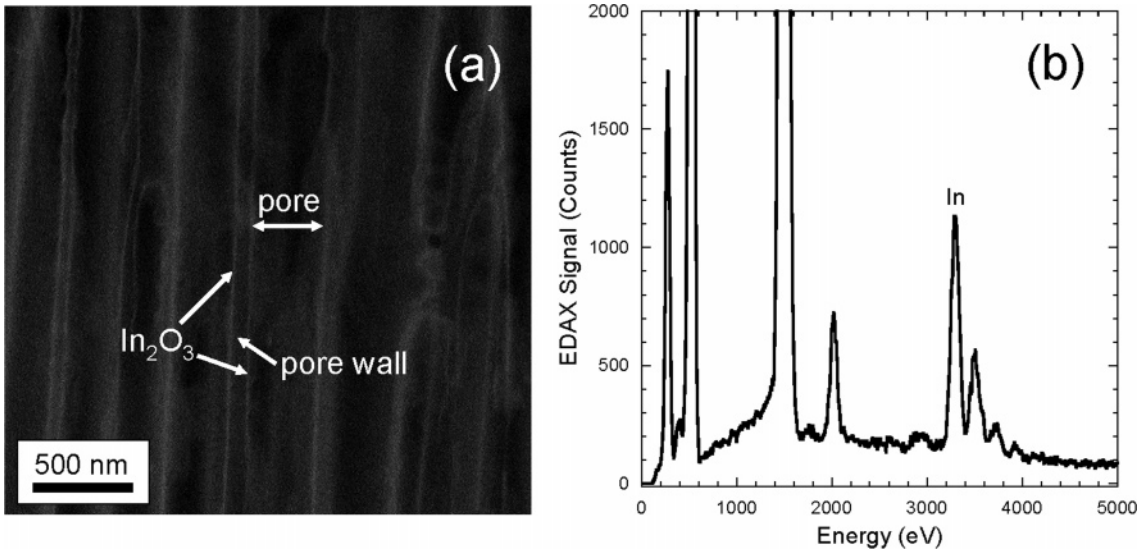

Figure 12. (a) Backscattered electron SEM image of a cross section of high aspect ratio AAO membrane with 13 nm ALD In_2O_3 coating deposited at 275 °C using the timing sequence 60−15−60−15. The white lines visible along the pore walls are the In_2O_3 coating. (b) EDAX spectrum recorded from same location at the center of the AAO membrane as in part a.

Cross-sectional SEM images (not shown) demonstrate that the In_2O_3 films are dense and free of voids, pinholes, or cracks.

Figure 11 shows the optical transmission spectrum of a 173 nm thick In_2O_3 film deposited on glass referenced to the uncoated glass. The average transmission of the In_2O_3 film over the wavelength range 400−1000 nm is $T = 90.0\%$ and is comparable to ALD In_2O_3 films deposited previously using $InCl_3/H_2O$.[16] This film had a resistivity of 16×10^{-3} Ω cm which is somewhat higher than the value of $(3-6) \times 10^{-3}$ Ω cm obtained using $InCl_3/H_2O$,[16] suggesting that the O_3 used in our process produces a more perfect In_2O_3 stoichiometry with fewer oxygen vacancies resulting in increased resistivity.

(E) In_2O_3 ALD in AAO Membranes. Next, we coated AAO membranes with In_2O_3 using 80 InCp/O_3 cycles at 250 °C. The AAO had an initial pore diameter $d = 200$ nm and thickness $L = 70$ μm such that the aspect ratio is $L/d = 350$. To allow gaseous diffusion of the precursors into the high aspect ratio pores, relatively long ALD cycle times of 60−15−60−15 were used.[24] Figure 12a shows a backscattered electron image recorded from the middle of a cleaved cross section of the AAO membrane. The white lines visible on the edges of the AAO nanopores are the In_2O_3 coating and appear brighter than the surrounding Al_2O_3 because the higher-Z indium backscatters electrons more efficiently. Because this sample was polished prior to imaging, the white lines are not likely caused by edge contrast. In fact, the pore structure was practically invisible in secondary electron images (not shown). Figure 12b shows an EDAX spectrum taken from the same location at the center of the AAO membrane, and the prominent In Lα peak at 3.29 keV demonstrates that the ALD In_2O_3 completely infiltrates the high aspect ratio AAO membrane. The intensity of the In Lα peak decreases by only 20% between the edge and the middle of the membrane, indicating very high conformality of the ALD In_2O_3 coating. We also coated much higher aspect ratio AAO membranes ($L/d = 2300$) using an identical treatment, but the coating was less conformal and the In Lα signal decreased by ∼90% between the edge and the middle of the membrane. This is most likely due to a decrease in concentration of the O_3 or oxygen radicals along the very high aspect ratio pores.

4. Conclusions

We have presented a method for preparing In_2O_3 films by ALD using alternating exposures to cyclopentadienyl indium(I) and ozone. This method yields a growth rate of 1.3−2.0 Å/cycle over the temperature range 200−450 °C using a precursor evaporation temperature of only 40 °C. In situ measurements reveal a mechanism in which approximately one in six of the initial Cp ligands remain on the surface following each InCp exposure, and the remaining Cp ligand is burned off during the subsequent O_3 exposure to form CO_2. The reactive sites for InCp adsorption are likely to be OH groups formed during the preceding oxidation step, and the active oxidizing species is believed to be oxygen radicals formed by O_3 thermal decomposition on the growing surface. The resulting films are nanocrystalline, cubic In_2O_3 that is highly transparent and conducting. Using this method, we demonstrate for the first time the conformal coating of very high aspect ratio porous membranes with ALD In_2O_3. This technique will enable the functionalization of porous materials with In-based TCO films for the fabrication of novel photovoltaic devices.

Acknowledgment. The work at Argonne is supported by the U.S. Department of Energy, BES-Materials Sciences, under Contract No. W-31-109-ENG-38. The work at Northwestern University is supported by the U.S. Department of Energy, Basic Energy Sciences Program, under Grant DE-FG02-87ER13808, and by the Link Foundation (graduate Fellowship for A.B.F.M.).

CM060754Y